Peer Reviewed Paper openaccess Paper Presented at IASIM 2016, July 2016, Chamonix, France

Can attenuated total internal reflection-Fourier transform infrared be used to understand the interaction between polymers and water? A hyperspectral imaging study

S. Mukherjee,[a,*] J.A. Martínez-González,[a] C.P. Stallard,[b] D.P. Dowling[b] and A.A. Gowen[a]

[a]School of Biosystems and Food Engineering, University College Dublin, Belfield, Dublin 4, Ireland. E-mail: sindhuraj.mukherjee@ucdconnect.ie

[b]School of Mechanical and Materials Engineering, University College Dublin, Belfield, Dublin 4, Ireland

This study investigates the potential use of attenuated total internal reflection-Fourier transform infrared (ATR-FT-IR) imaging, a hyperspectral imaging modality, to investigate molecular level trends in the interaction of water with polymeric surfaces of varying hydrophobicity. The hydrophobicity of two categories of polymeric biomaterials is characterised using contact angle (CA) measurements and their relationship with the band area of the OH stretching $\bar{\nu}_s$ vibration of water over time is presented. This is supported with correlations between CA data and single wavenumber intensity values (univariate analysis). Multivariate analysis of the spectra captured at the OH stretch for all polymers is carried out using principal component analysis to study the spatial variation in the interaction between the polymeric surfaces and water. Finally, a comparison between the univariate and multivariate strategies is presented to understand the interaction between polymeric biomaterials and water.

Keywords: ATR-FT-IR, polymer, HMDSO, hydrophobicity, silicon, water, hyperspectral imaging, wetting

Introduction

Polymeric biomaterials are widely used in different applications for example, in packaging,[1] pharmaceuticals,[2] medical devices and implants.[3] The surface properties of such polymeric biomaterials influence phenomena such as permeability, hydrophilicity,[4] diffusion, protein adsorption,[5] biocompatibility and degradation.[6] These phenomena are also affected by the nature of the interaction between such polymeric biomaterials and water. For example, Tanaka *et al.*[7] hypothesised that specific water layers at the proximity of biomedical polymers such as poly(ethylene glycol), polyvinylpyrrolidone, poly(methylvinylether) in contact with blood determine the biocompatibility of these polymers by influencing the conformation of subsequently adsorbed proteins to allow certain moieties to bond with the surface, while exposing others to water for hydrogen bonding. Chen *et al.*[8] discussed the importance of surface hydration in biofouling and found that highly hydrated surfaces generally exhibit non-fouling behaviour. Chandler[9] and Bunkin *et al.*[10] have reported differences in water structure near hydrophobic moieties, but the nature of the interaction is not very well understood. It has been proposed that this

Correspondence
S. Mukherjee (sindhuraj.mukherjee@ucdconnect.ie)

Received: 3 August 2016
Revised: 23 March 2017
Accepted: 31 March 2017
Publication: 7 April 2017
doi: 10.1255/jsi.2017.a3
ISSN: 2040-4565

Citation
S. Mukherjee *et al.*, "Can attenuated total internal reflection-Fourier transform infrared be used to understand the interaction between polymers and water? A hyperspectral imaging study", *J. Spectral Imaging* **6,** a3 (2017). doi: 10.1255/jsi.2017.a3

interaction is conditioned by the formation of hydrogen bonds between the surface of the polymeric biomaterial and water.[9] In order to understand the behaviour and operational limitations of polymeric biomaterials in biological systems that are largely composed of water, it is desirable to understand this interaction further.[11]

In this work, attenuated total internal reflection-Fourier transform infrared (ATR-FT-IR) imaging was investigated to study the interaction between water and polymeric biomaterials with a wide range of hydrophobicity. The aim of the study was to investigate correlations between contact angle (CA) measurements with ATR-FT-IR imaging spectroscopic measurements of wetted polymers.

Materials and methods

Polymer samples and HMDSO-coated silicon samples

Three commercial test samples of polymers PTFE, PET (Mylar™) and UHMPE were obtained from CS Hyde Company (1351 N. Milwaukee Avenue, Lake Villa, Illinois, USA), and characterised for hydrophobicity. From this point onwards in the manuscript, these commercial polymers samples are referred to as "bulk polymers".

Hexamethydisiloxane (HMDSO) coatings were polymerised using a modified plasma enhanced chemical vapour deposition technique developed at UCD's School of Mechanical and Materials Engineering, as described in more detail in a previous paper.[12] Films were deposited onto silicon wafers, resistivity 0–100 MΩ cm (450 µm thick) supplied by PI-KEM Ltd using an atmospheric pressure plasma jet. Prior to film deposition the wafers were ultrasonically cleaned in methanol, followed by acetone and propanol, air dried and pre-treated with He/O_2 plasma. The films were deposited from HMDSO (Aldrich ≥99.5%) using deposition conditions aimed at forming films with a range of water CAs. The deposition conditions used to deposit hydrophilic, hydrophobic and superhydrophobic films have previously been carried out with a system explained in a different article.[5] Deposition conditions used in this study are given in Table 1.

All samples were stored in sealed petri dishes at room temperature for up to four months (bulk polymers) and six months (HMDSO-coated wafers). For each polymer group studied, the same sample was tested at each time point.

Contact angle measurements

The hydrophobic effect of each material surface was quantified via water CA measurements, using the sessile drop technique.[13] This technique measures the level of hydrophobicity of a material surface based on the balance of interfacial free energies presented by a three-phase boundary system when the liquid comes in contact with a solid surface under ambient conditions.[14] Water CA measurements were recorded at three separate spatial locations in the central region of each sample using a Dataphysics™ OCA-20 goniometry system under room conditions.

The hydrophobic behaviour of HMDSO-coated wafers over time was studied by comparing a control set (kept in a sealed box at room conditions) and an experimental set (hydrated and used to collect experimental data). Bulk polymers behaviour was assumed to be stable at room conditions.

The HMDSO monomer was used to deposit nanometre thick coatings with a range of wetting properties. In the case of each coating, the monomer chemistry used was the same. Modification of hydrophobicity was achieved by altering deposition process conditions to slightly alter either the surface chemistry or surface roughness of the coatings. This warranted its own investigation, whereas, the bulk polymers' hydrophobicity is based on chemical differences and probably roughness as well.

Table 1. Deposition conditions and measured CA of plasma polymerised HMDSO films.

HMDSO film	Monomer flow rate ($\mu L\,min^{-1}$)	Plasma gas composition	Measured CA (24 h after deposition)
Hydrophilic	25	He, N_2, O_2	5
Hydrophobic	25	He, N_2	105
Superhydrophobic	5	He, N_2	150

Gas flow rates He: 5 slm, N_2: 0.70 slm, O_2: 0.25 slm. Plasma discharge power: 7.5 W

ATR-FT-IR scan acquisition

A Thermo Scientific™ Nicolet™ iN™10 infrared microscope (10× magnification, mercury-cadmium-tellurium detector, working range 7800–650 cm^{-1} with a 4 cm^{-1} spectral resolution) was used with a germanium crystal (refractive index = 4) to collect all ATR-FT-IR spectra. This system is fitted with two types of detector, a point detector, which collects spectra pixel by pixel, and an array detector, which collects spectra over a collection of points or pixels, before moving onto the next spatial location resulting in a higher speed of collection. Initially the array detector was used to collect hyperspectral images; however, after the second month of data collection, we found that the array detector produced noise in the spectral collection which was difficult to remove. Therefore, we decided to use the point detector for the rest of the spectral collection (i.e. Months 3–6). Additionally, spectral data from the third month of the HMDSO wafers dataset had to be removed due to a problem with the analysis of the superhydrophobic sample.

All spectra collected were combined in a data matrix called a "data cube" where each pixel of the data cube contains a specific spectrum from the polymeric biomaterial. The pixel sizes for data cubes captured by the point detector and array detector were 100 µm × 100 µm and 25 µm × 25 µm. The data cubes captured using the array detectors had a step size of 375 µm × 75 µm, whereas the data cubes captured with the point detector had a step size of 100 µm × 100 µm. This arrangement gave various sized areas captured by the two detectors. The number of spectra at Month 1 was 130 for PET (13 × 10), 91 for PTFE (13 × 7) and 169 for UHMPE (13 × 13). For Month 2, 793 spectra (13 × 61) were collected for each polymer and for subsequent months 100 spectra (10 × 10) were obtained for each polymer. The images extracted from data cubes were scaled to the same size by using the autoscaling option in the Matlab figure properties editor to provide a visual comparison between the differently sized images.

ATR spectra of the dry and wetted polymers were obtained. Wetted polymer spectra were captured after hydrating the polymers at room temperature with an equilibration time of at least 30 minutes by trapping water using BluTack™ to construct a well on the surface. Deionised (DI) water was used to wet the polymers, sourced from a Thermo Scientific™ Barnstead™ Smart2Pure™ water purification system (water Type I ASTM, resistance is 18.2 MΩ cm at temperature 25.6°C).

Data analysis

Water shows two characteristic spectral features in the mid-infrared, i.e. the OH bending vibration, $\bar{\nu}_B$, around 1640 cm^{-1} and the OH stretching vibration, $\bar{\nu}_S$, between 3800 cm^{-1} and 3000 cm^{-1}.[15,16] Both bands could serve as candidates to study how the interaction between biomaterials and water affects the formation of hydrogen bonds. We selected the OH $\bar{\nu}_S$ band because some rotational–vibrational polymer bands appear at the same region as the OH $\bar{\nu}_B$ vibration band (shown in Figure 1). Also, Tassaing *et al.* found that greater changes occur in the OH $\bar{\nu}_S$ region as compared to the OH $\bar{\nu}_B$ region when analysing the mid-IR spectra of supercritical water at different pressures,[17] suggesting that the OH $\bar{\nu}_S$ region is more sensitive to hydrogen bonding between water molecules.

The imaging spectra of two categories of polymeric biomaterials tested, i.e. bulk polymers and HMDSO-coated wafers, were concatenated separately into two different larger data matrices, one for bulk polymers and the other for HMDSO coatings. The spectra for each polymer was extracted from these normalised cubes and averaged to obtain a mean spectrum for each material sample. The matrices were further subsetted to extract the OH $\bar{\nu}_S$ region and subjected to standard normal variate normalisation or standard normal variate (SNV)[18] in order to minimise spectral variations arising from morphology of the samples.

The Pearson correlation coefficient[19] between the intensity of SNV-treated mean spectra of the OH $\bar{\nu}_S$ region and the mean value of the CA was calculated to study the relationship between the OH $\bar{\nu}_S$ region and the hydrophobicity. The significance of the correlation coefficients was determined by calculating the probability value (p-value) for accepting or rejecting the null hypothesis at a 5% level of significance. The null hypothesis here refers to no correlation between the two variables: intensity of SNV-treated mean spectra at a specific wavenumber of the OH $\bar{\nu}_S$ region and the mean value of the CA.

The wavenumber within the OH $\bar{\nu}_S$ vibration region showing the highest Pearson correlation coefficient was selected and the spatial variation in wetting of the polymeric surfaces at this particular wavenumber was visualised. The experimental OH $\bar{\nu}_S$ band is a combination of the symmetric and asymmetric stretch; and changes in the hydrophobicity of the polymeric biomaterial could be related to change in the intensity or position of the bands. Therefore, the band area of the OH $\bar{\nu}_S$ region was

also extracted from the SNV-treated mean spectra and compared to the CA to further investigate the response of the IR spectra of the wetted surfaces to changes in hydrophobicity.

Principal component analysis (PCA)[20] was carried out to visualise variation in the ATR-FT-IR imaging spectra of the wetted biomaterials studied. The OH $\bar{\nu}_S$ region was extracted from the data matrix containing combined imaging spectra for each category of polymeric biomaterial and subjected to SNV treatment. Then PCA was applied, and the variance explained by each principal component (PC) was calculated. Each PC is a summary of the variation in a dataset and is independent of other PCs. Score images of relevant PCs were analysed to visualise the spatial variation. The Pearson correlation coefficient between the average PC score values and CA of the polymeric biomaterials was also calculated to identify the most highly correlated PC with the CA measurement. Last, the score values of this PC were plotted as a function of the CA of the polymeric biomaterials and compared against the band area of the OH $\bar{\nu}_S$ region.

The CA data were analysed using Origin 9.0 (OriginLab®, Northampton, MA) and all spectral treatment and analysis was carried out using Matlab (Matlab 2014b, The MathWorks Inc., Natick, MA, 2000).

Results and discussion

Contact angle measurements

The CA data of the bulk polymers (Table 2) indicate their hydrophobic nature as well differences in measured hydrophobicity at different spatial locations.

According to the CA data collected, the hydrophobicity of the bulk polymers increased in this order: Mylar (PET), UHMPE and PTFE, consistently at all time points.

Some differences in spatial variation of the CA were noted. Variations in CA data measurements are expected at the different spatial locations over time, since CA data collected at the first location for Month 1 are not the same as those at the first location for the rest of the months for each polymer. It should also be noted that it is necessary to keep the surface totally flat when the CA measurement is obtained. The effect of fixing the sample at different positions to obtain a surface as flat as possible could explain the dispersion of the CA values for PET at Month 1. Finally, the protocol applied to collect CA and ATR-FT-IR measurements, repeated hydration and crystal pressure, may have affected the surface properties.

ATR-FT-IR results

The dry and wetted averaged spectra of the bulk polymers collected for the first month are presented in Figure 1. Spectral features of PET, UHMPE and PTFE are seen at 2000–1000 cm^{-1}, 3000–2500 cm^{-1} and 1500–1000 cm^{-1}, respectively. Spectral features of water, i.e. the OH $\bar{\nu}_S$ region (3800–3000 cm^{-1}) and OH bending band $\bar{\nu}_B$ (1640 cm^{-1}) are also visible in the wet spectra of the bulk polymers. As mentioned before, the OH $\bar{\nu}_S$ region, which is free from any overlap, was chosen for the analysis because the OH bend $\bar{\nu}_B$ overlaps with one of the native spectral feature of PET, (shown in Figure 1, upper section).

Non-pre-treated wet pixel spectra of the bulk polymers present great variations in the OH $\bar{\nu}_S$ region. Figure 2 shows this spectral variation for the entire spectral range as well as the OH $\bar{\nu}_S$ region. Such spectral variations are commonly encountered due to variations resulting from the array detector and sample morphology inherent to the bulk polymers. The OH $\bar{\nu}_S$ region spectra were normalised with SNV to reduce this spectral variation. The results of this pre-treatment are compared with the raw spectra in Figure 3.

The untreated or the wet raw spectra of the bulk polymers from all time points are presented in the upper section of Figure 3. The y-axis has been scaled so that the reader can visualise the spectral variation which was reduced on the application of the pre-treatment. The lower section shows the wet SNV-treated spectra

Table 2. CA data (mean value and standard deviation in degree) for the bulk polymers over four months stored in the laboratory (standard conditions).

	Month 1	Month 2	Month 3	Month 4
PET	86.95 ± 12.75	66.58 ± 9.83	72.69 ± 0.44	77.59 ± 2.31
UHMPE	87.91 ± 1.85	94.76 ± 4.58	95.53 ± 4.61	83.35 ± 2.48
PTFE	109.74 ± 9.97	131.12 ± 6.61	150.61 ± 3.81	128.87 ± 12.58

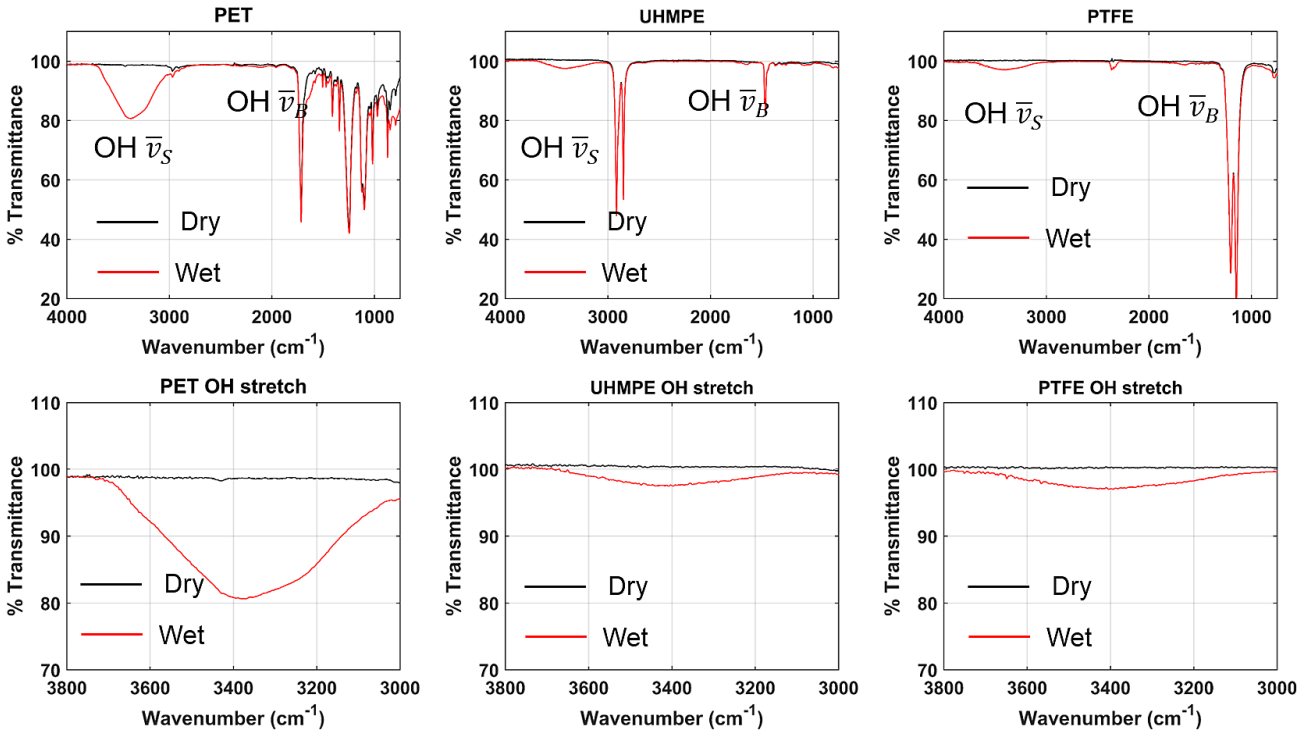

Figure 1. Raw dry (black line) and wet (red line) mean spectra from bulk polymers collected from the first month. Lower section focusses on the OH $\overline{v}_s$ region which is free from overlapping native polymer bands.

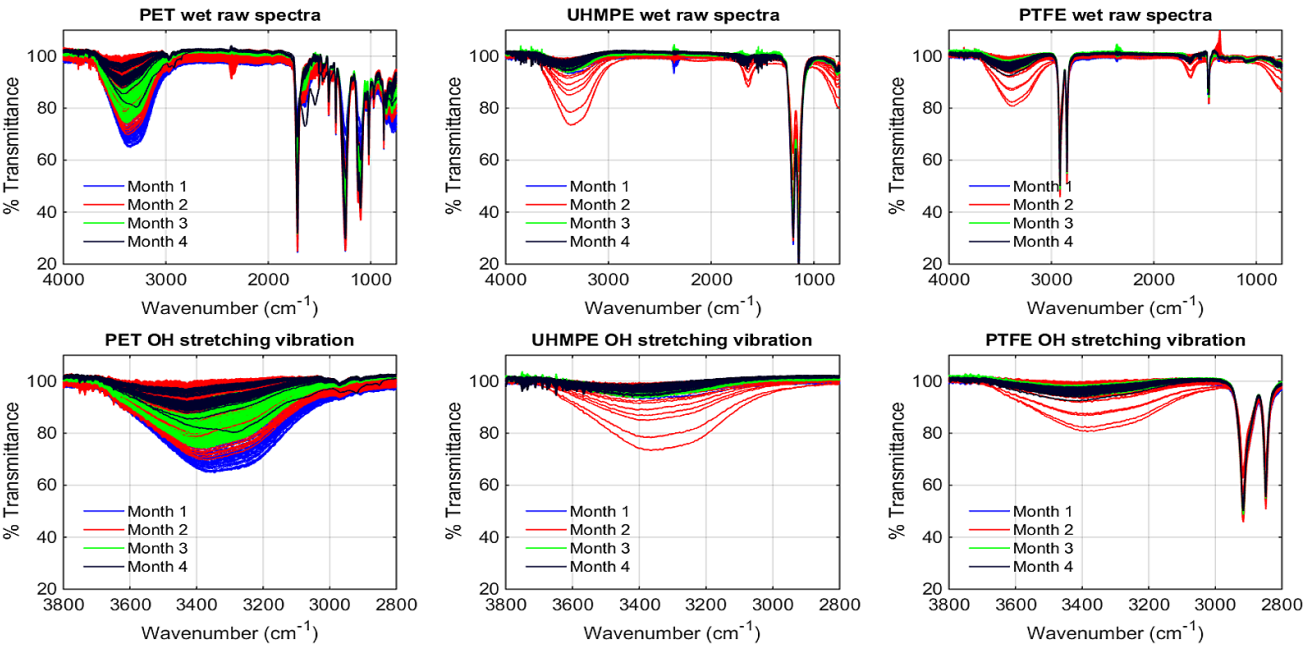

Figure 2. Raw (untreated) spectra of bulk polymers at all time points. Lower section focusses on the OH $\overline{v}_s$ region of wet spectra. Intense spectral variation is seen for Mylar (PET)—Month 1.

for the bulk polymers. While the spectral variation is reduced, the spectra collected for Month 1 and Month 2 show some noise in their spectral features. This is mostly likely due to the noise attributed to the array detector which was used to collect data for the first two months.

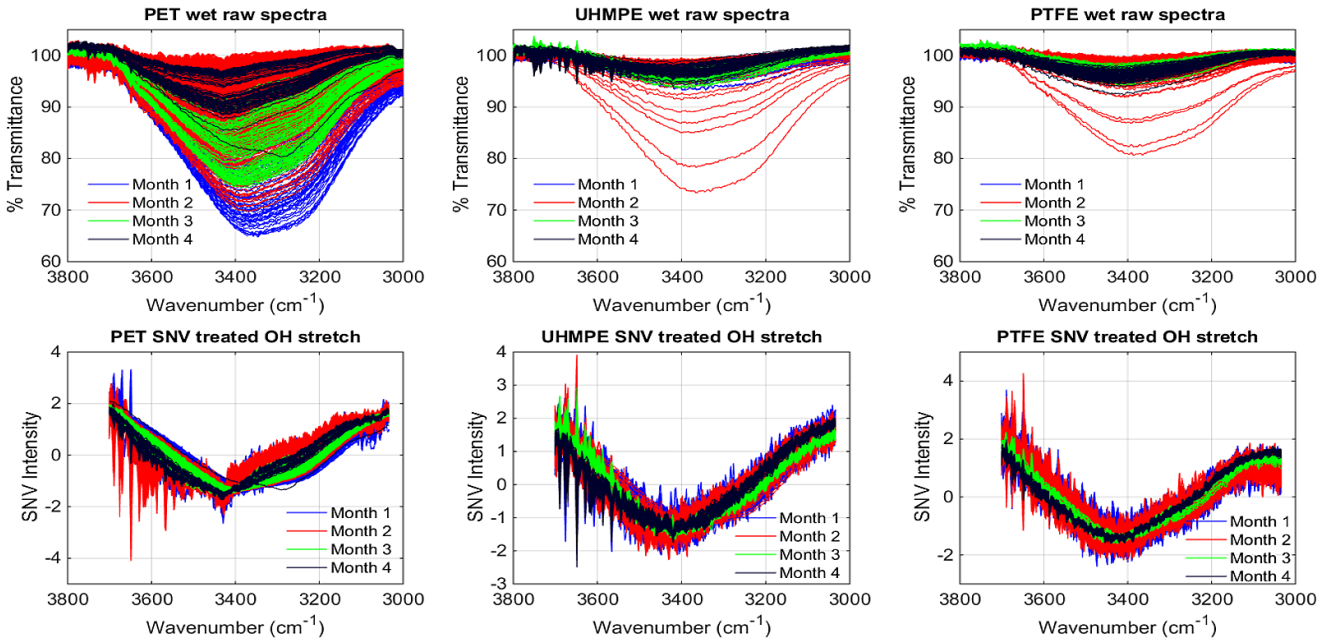

Figure 3. Effect of SNV normalisation on the OH $\bar{\nu}_S$ region for PET (left), UHMPE (centre) and PTFE (right) along the time. The top portion of the figure shows the untreated spectra, whereas the bottom portion shows the effect of the pre-treatment.

More hydrophobic polymers minimise water from spreading their surface.[9] Previously, the level of water absorption on a polyethylene glycol based pharmaceutical polymer[21] has been studied using the band area of the OH stretch. As part of this study we wanted to determine if this metric provides a good approximation to visualise the repulsion of water by the bulk polymers. The mean band area of the OH $\bar{\nu}_S$ over the four time points is presented in Table 3.

PET presented the largest variation in the band area for all months, as observed in Table 3. These variations could be compared with the CA data in Table 2. In both cases the variation was greatest for the first two months. For the two other polymers, UHMPE and PTFE, similar changes in the OH $\bar{\nu}_B$ band area were found. The data from Table 2 and Table 3 suggest that correlations could exist between the band area of the wavenumbers of the OH stretch region and the CA data. If any correlation exists, then the specific wavenumber(s) could be used to understand the interaction between polymeric biomaterials and water. The Pearson correlation coefficient was calculated between the band area of the SNV-treated mean spectra of the OH stretch for the bulk polymers and the CA data, and a low correlation coefficient value of −0.34 was found. This seemed to indicate that a weak decorrelation between the OH stretch band area and the CA data exists, i.e. as the CA (i.e. hydrophobicity) increases, the OH stretch band area increases. However, this required further investigation because the OH stretch represents almost 300 wavenumber variables and is composed of symmetric and asymmetric components. The Pearson correlation coefficient between the intensity of the SNV-treated mean spectra of each wavenumber of the stretching vibration and CA data for each polymer is presented in Figure 4.

Table 3. Values of the mean and standard deviation for the band area $\bar{\nu}_S$ region for the bulk polymers over time. The values are provided for comparison with Figure 3.

	Month 1	Month 2	Month 3	Month 4
PET	6635 ± 3471.64	2611.72 ± 1905.29	7211.81 ± 1691.57	3092.28 ± 1076.54
UHMPE	738.13 ± 118.63	895.57 ± 441.48	1531.17 ± 252.94	1512 ± 263.96
PTFE	960 ± 324.268	1041.32 ± 457.07	1869.53 ± 241.31	1625 ± 225.81

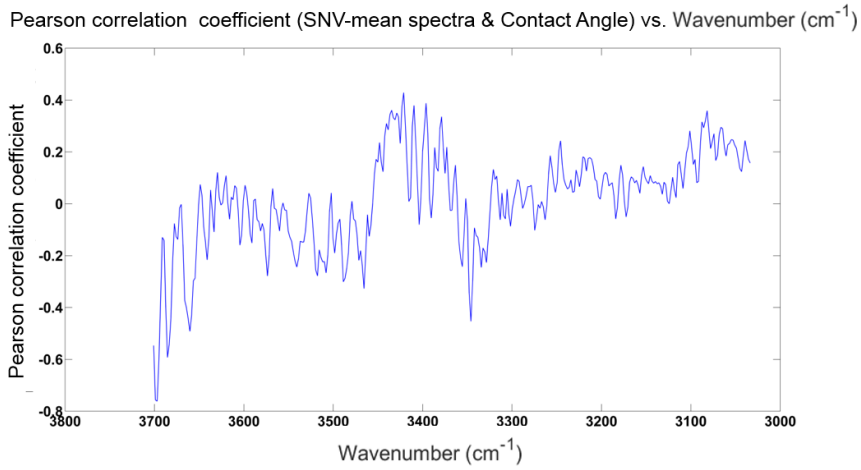

Figure 4. Pearson correlation coefficient between the intensity of the SNV-treated mean spectra of each wavenumber of the stretching vibration and CA data of each polymer. The wavenumber at 3697 cm^{-1} shows a relatively high correlation coefficient (−0.76).

The results show that the highest negative correlation between the wavenumbers of the stretching vibration and CA was found at 3697 cm^{-1} with a value of −0.76 (p-value = 0.0040). The significance of this correlation coefficient was determined by calculating the probability value (p-value) at a 5% level of significance. The null hypothesis here refers to no correlation between the two variables (i.e. intensity of SNV-treated mean spectra of the OH $\overline{\nu}_s$ region and the mean value of the CA of the bulk polymers). Since the p-value (0.0040) at 3697 cm^{-1} is less than the 5% significance level (p = 0.05), we accept our alternate hypothesis, i.e. the correlation coefficient at this wavenumber is significant.

In previous studies on metallic oxides (Al_2O_3 and TiO_2) and lipid membranes, 3697 cm^{-1} was associated with the presence of dangling[22] or disturbed[23] hydrogen bonds as a response to the hydrophobicity of the surface. It is reasonable to assume that a hydrophobic surface would disturb hydrogen bonding between the surface and water, which is what our correlation analysis indicates, i.e. as the CA of the surface increases, the intensity of the feature at 3697 cm^{-1} becomes less (shown in Figure 5). The weakness of the correlation, however, should be pointed out. This may be related to noise in the SNV-treated ATR-FT-IR spectra, as previously mentioned. Following this study the spatial variation of the interaction between water and bulk polymers was analysed at 3697 cm^{-1}.

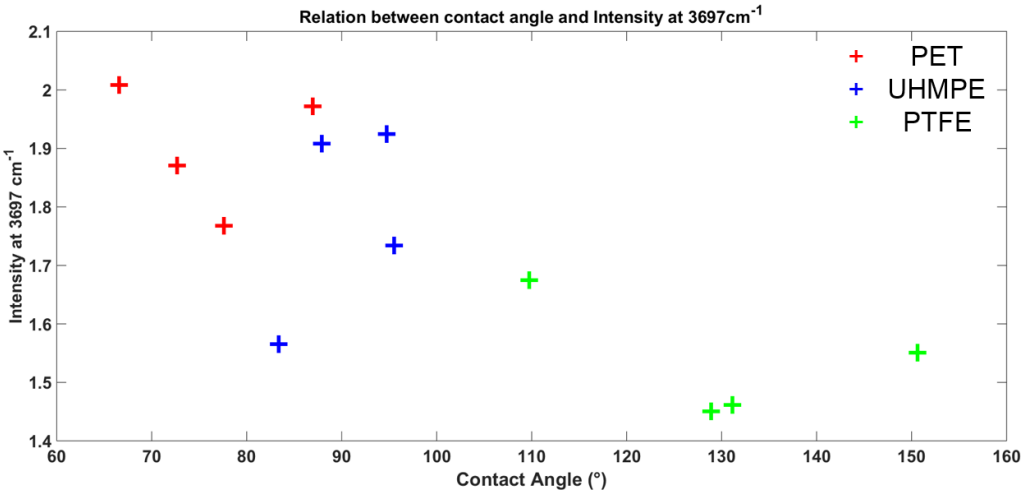

Figure 5. Absorption intensity at 3697 cm^{-1} (feature showing maximum correlation) plotted as a function of CA.

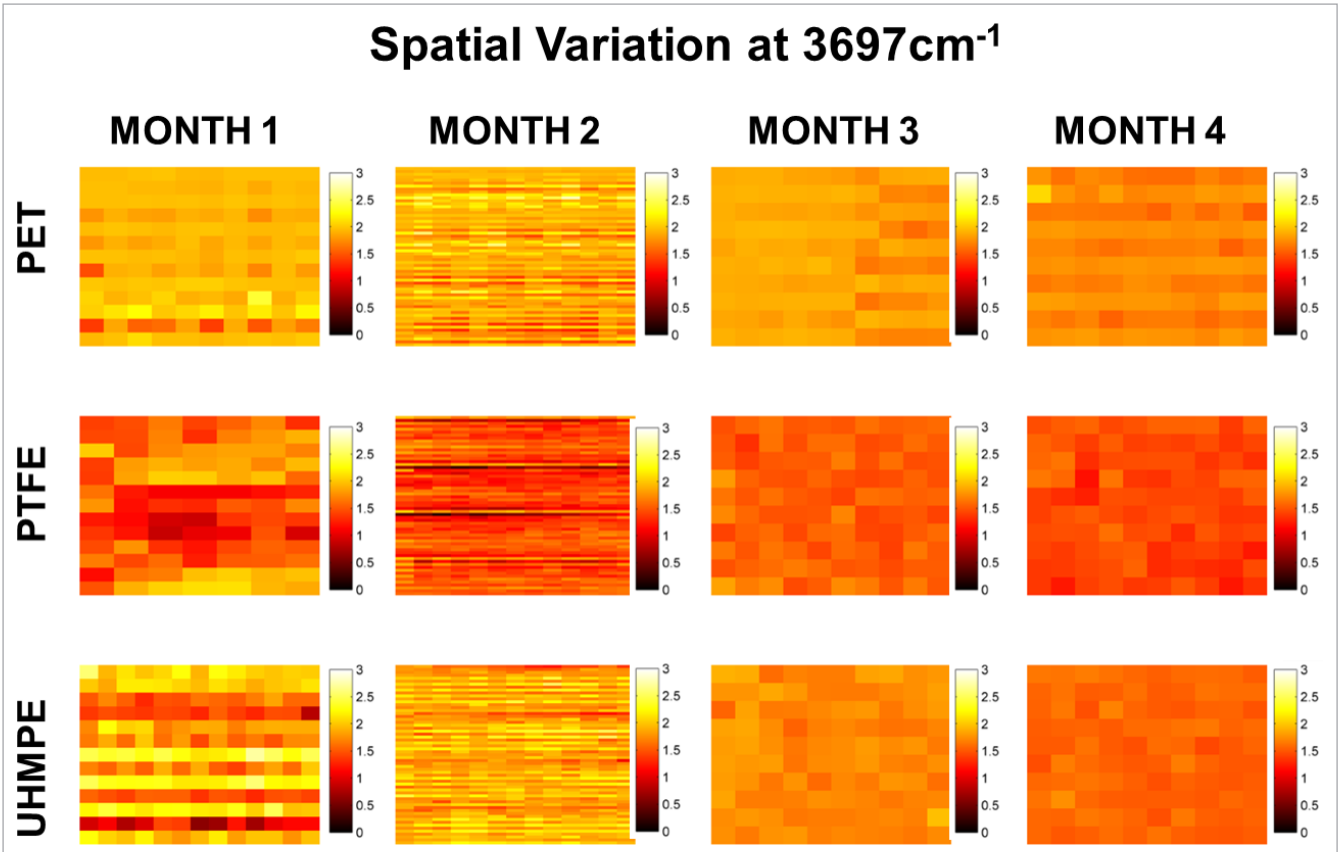

Figure 6. Spatial variation of % of transmittance intensity at 3697 cm^{-1} for PET (top), PTFE (centre) and UHMPE (bottom). A lighter pixel colour indicates higher % of transmittance intensity of the wavenumber 3697 cm^{-1} inferring lower hydrophobicity.

In Figure 6, the intensity of the SNV-treated imaging spectra at 3697 cm^{-1} for the bulk polymers over time is shown. Month 1 and Month 2 images show spatial variation occurring due to the noise presented by the array detector. Consistently, PTFE shows darker pixels, indicating a lower intensity of the wavenumber 3697 cm^{-1} at each pixel followed by UHMPE and PET. This can be compared to the contact angle data presented in Table 2, where PTFE shows the highest CA values followed by UHMPE and PET in decreasing order of hydrophobicity. A relationship between level of hydration and hydrophobicity has been found at this wavenumber, indicating the spectral feature at 3697 cm^{-1}, i.e. a univariate analysis with a single wavenumber image, could be used to visualise the interaction between water and a bulk polymer surface.

PCA results

The percentage variance accounted for by each PC is plotted in Figure 7. PC 1 accounted for 52% of the variance. This variation is most likely due to use of the two different detectors, as stated previously. Upon inspection of the PC 1 score images (right section, Figure 7), the variations due to the detector for Month 1 and Month 2 are clearer.

To investigate whether there was any correlation between PC scores and CA, the Pearson correlation coefficient was calculated between average PC score (averaged over each image) and CA. PC 11 had the largest absolute correlation coefficient (–0.55, p-value = 0.0040). On inspecting the loading plot of PC 11 (left section, Figure 8), a peak was found at 3690 cm^{-1} close to the spectral feature at 3697 cm^{-1} discussed previously. The score images for PC 11 for the bulk polymers are shown in the right section of Figure 8. The loading plots and score images of other PCs were also analysed, but PC 11 showed the highest Pearson correlation coefficient value. This feature most likely has a similar interpretation to that presented earlier, the presence of dangling or disturbed hydrogen bonds due

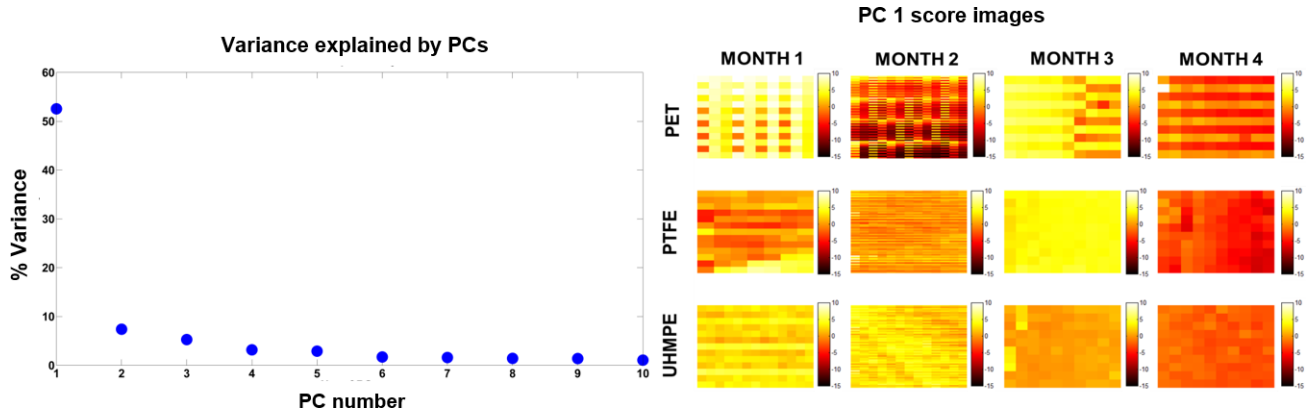

Figure 7. Variance explained by each PC (left). PC 1 accounts for almost 50% of the variation. Score images for PC 1 are shown in the right, where a lighter pixel colour indicates higher intensity of the PC score.

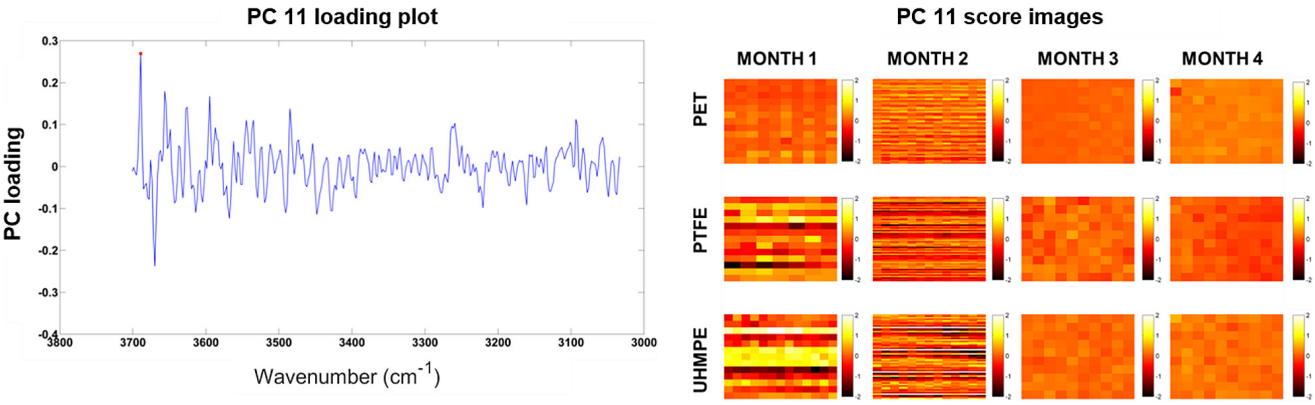

Figure 8. Loading plot for PC 11 (left) and spatial variation across PC 11 score images (right) for PET (top), PTFE (centre) and UHMPE (bottom) over time. Lighter colour of the pixel indicates higher intensity of the PC 11 loading prominent feature at wavenumber 3690 cm^{-1} inferring lower hydrophobicity for PET and UHMPE.

to the interaction of water with the surfaces of different hydrophobicity.

With PC 11 score images, it is quite difficult to see a consistent pattern or trend visualising the interaction between water and polymers. Month 4 PC 11 score image for PTFE shows darker pixels indicating higher hydrophobicity, whereas Month 1 for PTFE score images shows a higher number of lighter pixels. This might be explained by the fact that the polymer surfaces exhibit a heterogeneous nature of hydrophobicity, as seen in differences for CA for individual polymers in Table 2 which is reflected in the score images in Figure 8.

A comparison between the use of band area of the OH stretch and the use of PCA to explore the variation in the OH $\bar{\nu}_s$ region can be visualised in Figure 9. The left part of this figure shows the average PC 11 scores for all the polymers over time plotted as a function of CA. The right section of the figure shows the relationship between the OH $\bar{\nu}_s$ band area for the bulk polymers over time and the CA. While bulk polymers with a high hydrophobicity show a lower value of average PC 11 scores, this trend deviates for UHMPE data when comparing the OH $\bar{\nu}_s$ band area.

HMDSO-coated silicon wafers

The CA data for the control and experimental sets of the HMDSO-coated silicon wafers are shown in Table 4 and Table 5, which indicate that all the experimental HMDSO-coated wafers reach a similar state of hydrophobicity (80–100°) after five months. The control sets tended to maintain their hydrophobic properties better, but the hydrophilic coating increased in hydrophobicity after the first month, indicating that precautions such as removal of dust with compressed air and minimising contact with

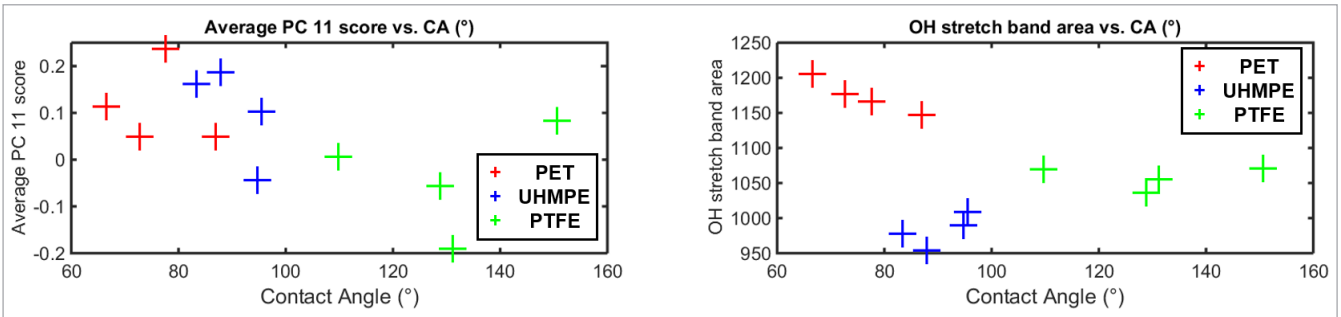

Figure 9. Comparison of average PC 11 scores (left) and OH stretch band area (right) as a function of CA for PET (red), UHMPE (blue) and PTFE (green) over time.

Table 4. CA data (mean value and standard deviation in degrees) for the control set of HMDSO-coated silicon wafers over four months.

	Month 1	Month 2	Month 4	Month 5
Hydrophilic	5 ± 0	47.18 ± 0.07	54.30 ± 1.11	57.85 ± 0.89
Hydrophobic	111.33 ± 0.44	103.1 ± 1.67	111.33 ± 1.65	102.90 ± 2.11
Superhydrophobic	156 ± 0	140.27 ± 0.04	150.32 ± 1.92	148.28 ± 2.60

Table 5. CA data (mean value and standard deviation in degrees) for the experimental set of HMDSO-coated silicon wafers over four months.

	Month 1	Month 2	Month 4	Month 5
Hydrophilic	5 ± 0	53.99 ± 7.95	74.15 ± 5.51	78.63 ± 4.69
Hydrophobic	109 ± 0	100.33 ± 5.33	109.10 ± 1.07	101.54 ± 4.23
Superhydrophobic	174.33 ± 0	100.76 ± 8.93	90.78 ± 4.42	102.42 ± 3.30

the surface must be taken while handling the hydrophilic-coated wafer. It is also well established that hydrophilic plasma polymers and plasma-treated polymers tend to recover their hydrophobicity over time,[24,25] and this can also be accelerated due to water diffusion into the interface.[26] In the case of experimental sets, the protocol used to collect the CA and ATR-FT-IR spectra increases the rate of this recovery. Also, repeated handling was likely associated with damage to the nano-structured morphology[12] of the superhydrophobic layers as the ATR crystal exerts pressure on the HMDSO-coated wafers (Table 4).

On further examination of the relationship between CA data of the HMDSO-coated wafers and the OH $\bar{\nu}_s$ band area, we found no consistent trend (Table 6). Coatings with similar hydrophobicity have a similar OH $\bar{\nu}_s$ band. This is probably reflective of the similarity of the hydrophobic coatings over time as indicated by CA data for the experimental HMDSO set in Table 5, which is contributed to by repeated testing on the same sample.

The Pearson correlation coefficient between the SNV-treated mean spectra for all the HMDSO-treated wafers and mean CA data as a function of wavenumbers in the OH $\bar{\nu}_s$ region is presented in Figure 10.

Although we stress that the individual Pearson correlation coefficients were very low, the highest relative values were observed at 3626 cm^{-1} and near 3200 cm^{-1} (3216 cm^{-1}, 3213 cm^{-1} and 3190 cm^{-1}), with a value for each one of –0.35, 0.37, 0.36 and 0.35, respectively. A peak at 3220 cm^{-1} has previously been reported to be related with hydrogen bond formation between water molecules on the Raman OH $\bar{\nu}_s$ band.[27] Therefore, these weak correlation coefficents could indicate a relationship between the wavenumbers of the OH $\bar{\nu}_s$ region and the hydrophobicity of the HMDSO-coated silicon wafers. The shift of the band near 3220 cm^{-1} could be due to the formation of some interaction between the water's

Table 6. Mean and standard deviation of OH $\bar{\nu}_s$ band area data for the experimental set of HMDSO-coated silicon wafers over four months.

	Month 1	Month 2	Month 4	Month 5
Hydrophilic	10329.59 ± 632.22	10422.57 ± 815.25	3205.88 ± 2138.38	10854.34 ± 557.84
Hydrophobic	10880.33 ± 242.88	10629.27 ± 800.20	10492.37 ± 760.58	10092.94 ± 2680.56
Superhydrophobic	9361.6 ± 343.81	12226.82 ± 244.65	9486.79 ± 2134.90	11661.24 ± 443

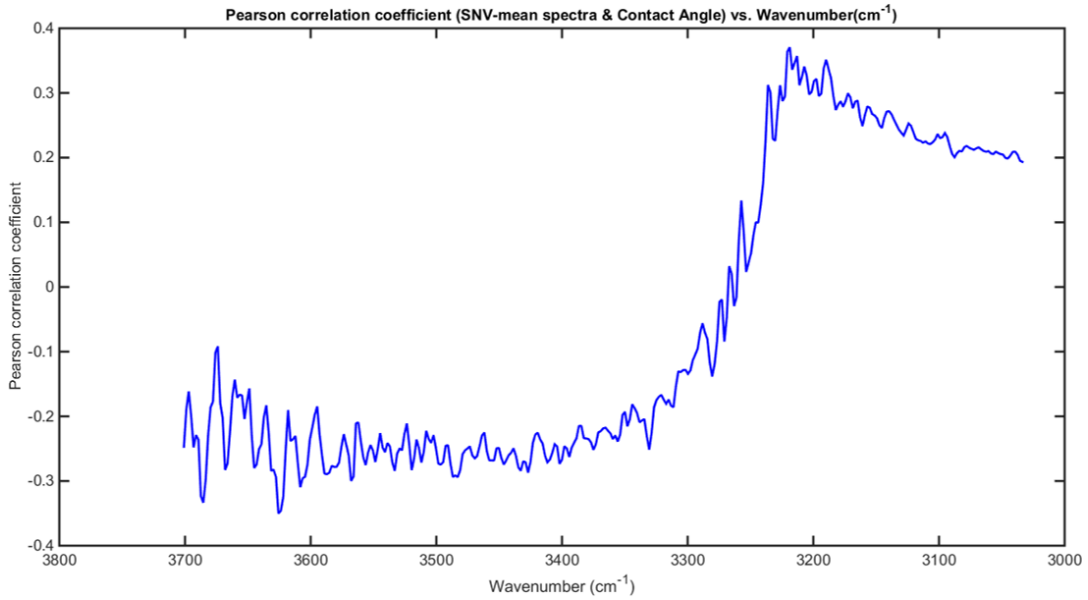

Figure 10. Pearson correlation coefficient calculated between SNV-mean spectra and CA data as a function of wavenumber (cm^{-1}). Very low correlation observed near 3200 cm^{-1}(0.35).

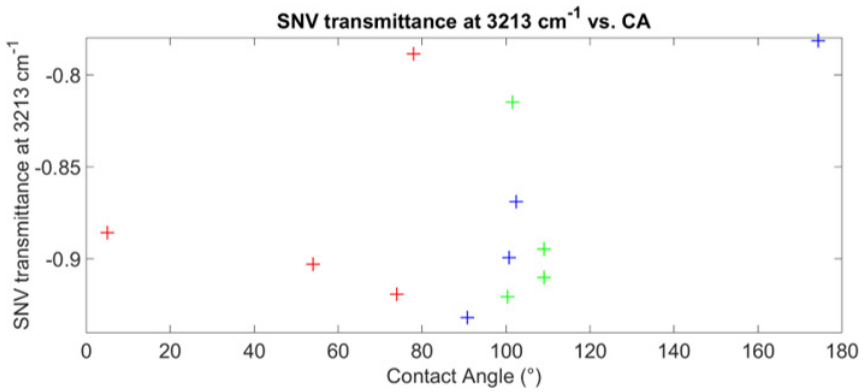

Figure 11. SNV transmittance at 3213 cm^{-1} as a function of CA data for HMDSO-coated Si wafers (red—hydrophilic, green—hydrophobic, blue—superhydrophobic).

hydrogen and the coating. In Figure 11, a trend cannot be found between the SNV-corrected absorbance at 3200 cm^{-1} and CA data for these coatings.

According to the calculated OH $\bar{\nu}_s$ areas for HMDSO wafers (Table 6), the value for the hydrophilic wafer at Month 4 appears to be very different when compared to the rest of the data. An explanation for this could be that the ATR crystal damaged the spatial region where the data was collected. In order to check whether this particular data point skewed the correlation between

CA and the intensity of the SNV-treated transmittance for wavenumbers in the OH $\bar{\nu}_S$ region, Hydrophilic-Month 4 data was removed from the data matrix and the Pearson correlation coefficient was recalculated. However, an analysis of the modified data matrix did not indicate a possible trend or explanation for this behaviour.

As with the bulk polymers, PCA on the SNV-treated OH $\bar{\nu}_S$ region of the HMDSO-coated silicon wafers was carried out and correlations between the PC scores and the CA data were calculated. A very low correlation (0.4, p-value = 0.2) was found for PC 7 and PC 13 but the p-value indicated that the correlation was not significant. Similarly, removal of hydrophilic-Month 4 data showed no improvement in the correlation coefficient between PC scores and CA data.

Conclusions

The interaction between polymers and water using ATR-FT-IR hyperspectral imaging was investigated, focussing on the OH stretching vibration $\bar{\nu}_S$ band region. We compared two categories of polymeric biomaterials, bulk polymers and HMDSO-coated silicon wafers. Using CA data, we characterised the hydrophobicity of the polymeric biomaterials and investigated the relationship between it and the OH $\bar{\nu}_S$ band region of the mid-IR. We found a significant correlation between the CA data of the bulk polymers and ATR-FT-IR spectra at 3697 cm^{-1} indicative of the disturbed or disrupted hydrogen bonding networks near such surfaces. Multivariate analysis of bulk polymers was carried out and the band area of the OH $\bar{\nu}_S$ region was also analysed. The results indicated a significant correlation between PC 11 scores and CA, while lower OH $\bar{\nu}_S$ band areas were observed for bulk polymers with a higher degree of hydrophobicity. This indicates that ATR-FT-IR imaging shows potential for studying interactions between bulk polymers and water.

However, HMDSO coatings in contact with water did not show a repeatable correlation between CA data and hydrated spectral features acquired through ATR-FT-IR imaging, likely due to ageing of the coatings and damage to the surface coatings due to repeated testing of the specimens.

Acknowledgements

The authors gratefully acknowledge funding from the EU FP7 under the European Research Council Starting Grant programme (ERC-SG-335508). This work was presented as part of IASIM 2016, Chamonix-Mt Blanc, France.

References

1. R. Auras, B. Harte and S. Selke, "An overview of polylactides as packaging materials", *Macromol. Biosci.* **4,** 835–864 (2004). doi: https://doi.org/10.1002/mabi.200400043
2. J. Khandare and R. Haag, "Pharmaceutically used polymers: principles, structures, and applications of pharmaceutical delivery systems", *Handbook of Experimental Pharmacology* **197,** 221–250 (2010). doi: https://doi.org/10.1007/978-3-642-00477-3_8
3. A.J.T. Teo, A. Mishra, I. Park, Y.-J. Kim, W.-T. Park and Y.-J. Yoon, "Polymeric biomaterials for medical implants and devices", *ACS Biomater. Sci. Eng.* **2,** 454–472 (2016). doi: https://doi.org/10.1021/acsbiomaterials.5b00429
4. D. Bhattacharyya, H. Xu, R.R. Deshmukh, R.B. Timmons and K.T. Nguyen, "Surface chemistry and polymer film thickness effects on endothelial cell adhesion and proliferation", *J. Biomed. Mater. Res. A* **94,** 640–648 (2010). doi: https://doi.org/10.1002/jbm.a.32713
5. C.P. Stallard, K. McDonnell, O.D. Onayemi, J.P. O'Gara and D.P. Dowling, "Evaluation of protein adsorption on atmospheric plasma deposited coatings exhibiting superhydrophilic to superhydrophobic properties", *Biointerphases* **7,** 31 (2012). doi: https://doi.org/10.1007/s13758-012-0031-0
6. I. Donelli, G. Freddi, V.A. Nierstrasz and P. Taddei, "Surface structure and properties of poly-(ethylene terephthalate) hydrolyzed by alkali and cutinase", *Polym. Degrad. Stab.* **95,** 1542–1550 (2010). doi: https://doi.org/10.1016/j.polymdegradstab.2010.06.011
7. M. Tanaka, T. Hayashi and S. Morita, "The roles of water molecules at the biointerface of medical polymers", *Polym. J.* **45,** 701–710 (2013). doi: https://doi.org/10.1038/pj.2012.229

8. S. Chen, L. Li, C. Zhao and J. Zheng, "Surface hydration: principles and applications toward low-fouling/nonfouling biomaterials", *Polymer (Guildf.)* **51,** 5283–5293 (2010). doi: https://doi.org/10.1016/j.polymer.2010.08.022
9. D. Chandler, "Interfaces and the driving force of hydrophobic assembly", *Nature* **437,** 640–647 (2005). doi: https://doi.org/10.1038/nature04162
10. N. Bunkin, P.S. Ignatiev, V.A. Kozlov, A.V. Shkirin, S.D. Zakharov and A.A. Zinchenko, "Study of the phase states of water close to Nafion interface", *Water J.* **4,** 129–154 (2013). doi: https://doi.org/10.14294/WATER.2013.1
11. E.A. Vogler, "Structure and reactivity of water at biomaterial surfaces", *Adv. Colloid Interface Sci.* **74,** 69–117 (1998). doi: https://doi.org/10.1016/S0001-8686(97)00040-7
12. C.P. Stallard, M.M. Iqbal, M.M. Turner and D.P. Dowling, "Investigation of the formation mechanism of aligned nano-structured siloxane coatings deposited using an atmospheric plasma jet", *Plasma Processes Polym.* **10,** 888–903 (2013). doi: https://doi.org/10.1002/ppap.201300056
13. D.Y. Kwok, T. Gietzelt, K. Grundke, H.-J. Jacobasch and A.W. Neumann, "Contact angle measurements and contact angle interpretation. 1. Contact angle measurements by axisymmetric drop shape analysis and a goniometer sessile drop technique", *Langmuir* **13,** 2880–2894 (1997). doi: https://doi.org/10.1021/la9608021
14. H.-J. Butt, I.V. Roisman, M. Brinkmann, P. Papadopoulos, D. Vollmer and C. Semprebon, "Characterization of super liquid-repellent surfaces", *Curr. Opin. Colloid Interface Sci.* **19,** 343–354 (2014). doi: https://doi.org/10.1016/j.cocis.2014.04.009
15. G. Socrates, *Infrared and Raman Characteristic Group Frequencies*. John Wiley & Sons (2004).
16. L.J. Bellamy, *The Infrared Spectra of Complex Molecules*. Chapman and Hall (1980). doi: https://doi.org/10.1007/978-94-011-6520-4
17. T. Tassaing, Y. Danten and M. Besnard, "Infrared spectroscopic study of hydrogen-bonding in water at high temperature and pressure", *J. Mol. Liq.* **101,** 149–158 (2002). doi: https://doi.org/10.1016/S0167-7322(02)00089-2
18. C. Esquerre, A.A. Gowen, J. Burger, G. Downey and C.P. O'Donnell, "Suppressing sample morphology effects in near infrared spectral imaging using chemometric data pre-treatments", *Chemometr. Intell. Lab. Syst.* **117,** 129–137 (2012). doi: https://doi.org/10.1016/j.chemolab.2012.02.006
19. J.L. Rodgers and, W.A. Nicewander, "Thirteen ways to look at the correlation coefficient", *Am. Stat.* **42,** 59–66 (1988). doi: https://doi.org/10.1080/00031305.1988.10475524
20. S. Wold, K. Esbensen and P. Geladi, "Principal component analysis", *Chemometr. Intell. Lab. Syst.* **2,** 37–52 (1987). doi: https://doi.org/10.1016/0169-7439(87)80084-9
21. K.L. Chan and S. Kazarian, "Visualisation of the heterogeneous water sorption in a pharmaceutical formulation under controlled humidity via FT-IR imaging", *Vib. Spectrosc.* **35,** 45–49 (2004). doi: https://doi.org/10.1016/j.vibspec.2003.11.005
22. M. Takeuchi, L. Bertinetti, G. Martra, S. Coluccia and M. Anpo, "States of H_20 adsorbed on oxides: an investigation by near and mid infrared spectroscopy", *Appl. Catal. A Gen.* **307,** 13–20 (2006). doi: https://doi.org/10.1016/j.apcata.2006.03.002
23. H. Binder, "Water near lipid membranes as seen by infrared spectroscopy", *Eur. Biophys. J.* **36,** 265–279 (2007). doi: https://doi.org/10.1007/s00249-006-0110-6
24. H. Hillborg, N. Tomczak, A. Ola, H. Scho and G.J. Vancso, "Nanoscale hydrophobic recovery: a chemical force microscopy study of UV/ozone-treated cross-linked poly(dimethylsiloxane)", *Langmuir* **20,** 785–794 (2004). doi: https://doi.org/10.1021/la035552k
25. D. Hegemann, H. Brunner and C. Oehr, "Plasma treatment of polymers for surface and adhesion improvement", *Nucl. Instrum. Meth. Phys. Res. B* **208,** 281–286 (2003). doi: https://doi.org/10.1016/S0168-583X(03)00644-X
26. M.M. Schäfer, C. Seidel, H. Fuchs and M. Voetz, "Suppression of water-diffusion in polycarbonate through Ar-and He-plasma as a new model for the origin of improved adhesion of Al", *Appl. Surf. Sci.* **173,** 1–7 (2001). doi: https://doi.org/10.1016/S0169-4332(00)00843-6
27. Q. Sun, "Raman spectroscopic study of the effects of dissolved NaCl on water structure", *Vib. Spectrosc.* **62,** 110–114 (2012). doi: https://doi.org/10.1016/j.vibspec.2012.05.007